

Journal of Biomedical Optics

BiomedicalOptics.SPIEDigitalLibrary.org

Penetration depth of focused beams in highly scattering media investigated with a numerical solution of Maxwell's equations in two dimensions

Ahmed Elmaklizi
Dominik Reitzle
Arnd Brandes
Alwin Kienle

Penetration depth of focused beams in highly scattering media investigated with a numerical solution of Maxwell's equations in two dimensions

Ahmed Elmaklizi,* Dominik Reitzle, Arnd Brandes, and Alwin Kienle

Ulm University, Institute of Laser Technologies in Medicine and Metrology, Helmholtzstrasse 12, D-89081 Ulm, Germany

Abstract. The propagation of different focused beams (e.g., Gaussian or quasi-Bessel beams) through scattering media is studied. The finite-difference time-domain method, a numerical solution of Maxwell's equations, is applied to propagate the light beams in two dimensions. The focused beams are modeled by applying the angular spectrum of the plane waves method. The results show that weakly focused beams exhibit comparable performance to strongly focused beams in delivering focused light deep into scattering media. © 2015 Society of Photo-Optical Instrumentation Engineers (SPIE) [DOI: [10.1117/1.JBO.20.6.065007](https://doi.org/10.1117/1.JBO.20.6.065007)]

Keywords: focused beams; finite-difference time-domain; scattering media; Maxwell's equations.

Paper 150150R received Mar. 13, 2015; accepted for publication May 28, 2015; published online Jun. 25, 2015.

1 Introduction

Focusing light deeply into scattering media is important in many research fields.¹⁻⁴ In biophotonics, it is used, e.g., for obtaining three-dimensional (3-D) microscopical pictures from tissue using established methods such as laser-scanning microscopy or multiphoton microscopy. There are several types of beams which are of particular interest due to their wide spread applications, e.g., a Gaussian beam,⁵ a Bessel beam,⁶ and a sinc-function type beam,⁷ which is called a focused beam within this manuscript. The Gauss beam is used in many fields of science since it models the fundamental laser mode (the lowest mode of an optical cavity).^{5,8} A common application for the Bessel beam is light sheet microscopy.^{9,10} Most of the studies done on the Bessel beam were either concentrating on the propagation of the beam itself *in vacuo* and the manipulation of its properties^{6,11-13} or on the interaction between that beam and the scattering media. Those studies have been either experimental or used an approximated numerical solution such as the beam propagation method^{14,15} (BPM). In this work, a quasi-Bessel beam is simulated in two-dimensions (2-D). This is different from a Bessel beam which cannot be simulated in 2-D due to the loss of the third dimension, which makes it impossible to use cylindrical symmetry. Finally, the focused beam, as it is called here, is interesting because it is obtained when an objective is over-illuminated by a homogeneous extended source (plane wave illumination) delivering a highly focused beam.^{7,16,17}

In previous works, numerical solutions of Maxwell's equations were used to generate a focused beam by applying the angular spectrum of plane waves method (ASPW).¹⁶⁻¹⁸ This solution proved to be adaptable to many beam profiles. For example, the Bessel beam was modeled using the ASPW, but was computed with the BPM.^{9,10,19}

In this work, the interaction between the incident light and the scattering media is examined for the different beam profiles using a numerical solution of Maxwell's equations. It is shown that a less focused beam shows a similar performance compared to a highly focused one in delivering focused light deep into the scattering medium. The numerical simulations are performed using the finite-difference time-domain (FDTD) method. These simulations are carried out in 2-D due to the lower demand on the computational performance compared to calculations in 3-D. Moreover, in order to compare the penetration depth for each beam, the respective beam is scanned through the scattering media using a recently developed postprocessing method,¹⁷ which is also applied to smooth the interference effects.

2 Theory

2.1 ASPW Method

The ASPW approach is applied to model the light propagation of different focused beams. The ASPW describes the optical fields of the focused beams as a superposition of propagating plane waves.²⁰ In brief, first the spatial distribution of the electric field $E(x=0, y)$ in the focal plane is given. Then using a Fourier transform, the electric field versus spatial frequency $\hat{E}(k_y)$ is calculated. By substituting the integrands in the Fourier transform, the angular description $\hat{E}(\theta)$ in the far field is obtained.²¹ Following the work of Richards and Wolf, we model the focusing effect by the usage of an aplanatic lens. Thus, we need to take the geometric intensity law into account.⁷ After these mathematical manipulations, we write the spatial electric field as a function of the angular far field in a discretized form to facilitate the simulations later on using plane waves incident at discrete angles:

*Address all correspondence to: Ahmed Elmaklizi, E-mail: ahmed.elmaklizi@ilm.uni-ulm.de

$$E(x, y) = \sum_{m=1}^M \hat{E}(\theta_m) \exp[jk(x \cos \theta_m + y \sin \theta_m)] \sqrt{\cos \theta_m}, \quad (1)$$

where M is the number of plane waves used to model the beam and θ_m is the incident angle for the m 'th plane wave measured relative to the x -axis in the $x - y$ plane (see Fig. 1). The propagation direction in the 2-D case is the x -direction, whereas the y denotes the lateral direction. The electric field in the z -dimension is constant making the power infinite. Thus, we normalize all beams to a given differential power. Another advantage of performing the investigation in 2-D is the decoupling of Maxwell's equations into two sets of equations for two independent polarizations.²² In this study, we are concentrating on the parallel polarization ($E_x = E_y = 0$). Therefore, all electric field components are polarized in the z -direction. Thus, the subscript is suppressed.

2.2 Beam Scanning

In this paper, the main point of interest is the study of the deterioration of the beam focus while the mentioned focus is scanned through the scattering medium. Simulating a focused beam is achieved by using Eq. (1). Performing the simulation for many positions of the focus would take much more time. Here, we can use another advantage of the ASPW description of the beams. By performing the steady state simulation of each individual plane wave and saving the obtained fields separately, we can scan the beam through the medium by multiplying the saved data from a single simulation set by the appropriate phase shifts as explained in detail in our previous work.¹⁷ The complete solution of the scanned beam is calculated according to

$$E_{\text{shift}}(x, y) = \sum_{m=1}^M \hat{E}(\theta_m) \exp[jk(x \cos \theta_m + y \sin \theta_m)] \cdot \exp[jk(x_{\text{sh}} \cos \theta_m + y_{\text{sh}} \sin \theta_m)] \sqrt{\cos \theta_m}, \quad (2)$$

where E_{shift} is the steady state electric field for a longitudinal shift x_{sh} and a lateral shift y_{sh} of the focus position.

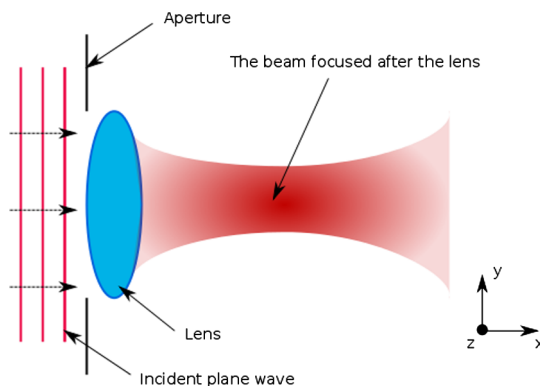


Fig. 1 Geometry of the simulations as carried out in this paper. The setup is infinite in z -direction. The electric field is propagating in the x direction while being polarized in z -direction. The dark region in the middle of the beam is to visualize the focusing effect after going through the lens.

2.3 Gaussian and Focused Beams

In order to obtain a focused beam, the angular distribution of the plane waves used in the ASPW has to be defined. We start with the electric field distribution of a Gaussian profile in the spatial domain:²³

$$E(x = 0, y) = E_0 e^{-\beta^2 y^2}, \quad (3)$$

where $1/\beta^2$ corresponds to the square of the beam waist and E_0 is the amplitude of the Gaussian beam. Knowing the distribution of the fields in space, we obtain the angular distribution by performing a Fourier transform. In the angular domain, we get

$$\hat{E}(\theta) = \frac{E_0}{2\sqrt{\pi}\beta} e^{-\left(\frac{k \sin \theta}{2\beta}\right)^2}, \quad (4)$$

which allows us to model the focal plane of a Gaussian beam. However, once the beam waist approaches the value of the wavelength ($1/\beta \approx \lambda$), Eq. (4) tends toward 1 delivering the so-called focused beam. Such a mathematical model is a good description for a plane wave passing through an aperture (top-hat profile in the angular spectrum), where the aperture is described by the maximum divergence angle allowed (θ_{max}).

2.4 Quasi-Bessel Beam

In 3-D, a Bessel beam can be generated by illuminating an annular aperture.¹³ Due to the loss of cylindrical symmetry (since the simulations are performed in 2-D), a quasi-Bessel beam²⁴ can be formed by the light incident from two angular ranges. To model this mathematically, we use the equation

$$\hat{E}(\theta) = E_0 \left\{ \text{rect} \left[\frac{2(\theta - \theta_{\text{max}}) + \Delta\theta}{2\Delta\theta} \right] + \text{rect} \left[\frac{2(\theta + \theta_{\text{max}}) - \Delta\theta}{2\Delta\theta} \right] \right\}, \quad (5)$$

where θ_{max} is the maximum divergence angle and $\Delta\theta$ is the angular width of the beam.

3 Simulations

3.1 FDTD Method

For the purpose of studying the focusing of light beams in scattering media in this work, the FDTD²⁵ method is used. This method solves Maxwell's equations in the time domain, providing the results over a wide range of frequencies in a single run. The method of total field-scattered field is used to inject the incident light into the simulation grid. It can be adapted to inject plane waves with different oblique angles, which are used in the ASPW method to generate the focused beams.¹⁶⁻¹⁸ The code applied in this paper has been verified and explained in more details elsewhere.²² Throughout this work, the resolution of the grid ($\Delta x, \Delta y$) used in the simulations is $\lambda/20$.

3.2 Scattering Media

The scattering medium is modeled as an ensemble of cylindrical scatterers which are randomly distributed²² in a matrix. The cylinders have a diameter (d) of $1 \mu\text{m}$ and are suspended in the matrix with a volume concentration of 30%. FDTD simulations

are carried out for three samples, which differ in the refractive index of the scatterers ($n_s = 1.4, 1.45$ and 1.5) while the refractive index of the matrix is kept constant at $n_m = 1.33$. The mean free path (ρ) for these scattering media²⁶ is $\rho = 21.98, 7.53$, and $3.84 \mu\text{m}$ when coherence effects, such as dependent scattering,²⁷ are ignored. In addition, for all the samples, the absorption of both the scatterers and the surrounding media is set to zero.

3.3 Illumination

Three types of beams are simulated as the illumination source: a focused beam, a Gaussian beam, and a quasi-Bessel beam. Due to the fact that all beams are formed using the ASPW method, we are able to reuse the intermediate results of the plane waves to calculate the respective ASPW solution of other beams. This is achieved by choosing the plane waves that correspond to the range of angles relevant to the beam of interest. For the focused beam, the maximum divergence angle amounts to $\theta_{\text{max}} = 15, 25, 45$ deg. These values are substituted in Eqs. (1) and (4) while taking the beam waist to be much smaller than the wavelength, which corresponds to the same weighting for all the plane waves that constitute the beam.

The Gaussian beam is simulated by choosing a beam waist of full width at half maximum (FWHM) = $0.86 \mu\text{m}$, which corresponds to an angle of 25 deg for the angular beam waist. For the quasi-Bessel beam, Eqs. (1) and (5) are applied with $\Delta\theta = 20$ deg and θ_{max} of 45 deg.

In all five cases, the wavelength (λ) is equal to $1 \mu\text{m}$. The number of plane waves used to form the beams is 161 in the range from 45 to -45 deg. Each of the beams is defined mainly by the range of angles that it has in the angular domain. So a focused beam with a maximum divergence angle of 45 deg

consists of plane waves in the range from -45 to 45 deg. This is written in short hand as $|\theta| = [0 \text{ deg} : 45 \text{ deg}]$.

4 Results

In Fig. 2, the intensity is shown when using a focused beam ($\theta_{\text{max}} = 45$ deg) at different focus positions, whereas in Fig. 3, the same is shown for the quasi-Bessel beam case ($\theta_{\text{max}} = 45$ deg, $\Delta\theta = 20$ deg). The two figures have been normalized to an incident differential power of 1 W/m in each case. In both cases, the scatterers have a refractive index of $n_s = 1.5$. It can be observed that certain transmission channels occur in the medium.²⁸

The main problem at this point is that due to interference, it is difficult to get a quantitative comparison between the simulated beams while propagating through different scattering media. Averaging over multiple randomly chosen distributions of scatterers is a possible solution to obtain a smoother dependence of the intensity versus spatial position. However, this increases the simulation time. A more efficient solution is to use the ASPW method and to scan the beam as explained in the theory sections. Here, the focus is scanned in the lateral direction ($\pm 20 \mu\text{m}$). Then we average the intensity from all of these lateral scans incoherently to obtain the averaged intensity for each depth. As an example, the averaging of the intensity in Figs. 2 and 3 can be seen in Figs. 4 and 5, respectively. To further enhance the averaged results, 10 randomly chosen distributions of scatterers were applied in addition to the usage of the beam scanning.

In Fig. 6, the on-axis intensity is shown for all beams after being scanned through the scattering medium having $n_s = 1.5$. It should be noted that the position of the maximal intensity of the beam (x_0) is different from the position without scatterers (\hat{x}_0). Thus, a correction term considering the refractive indices

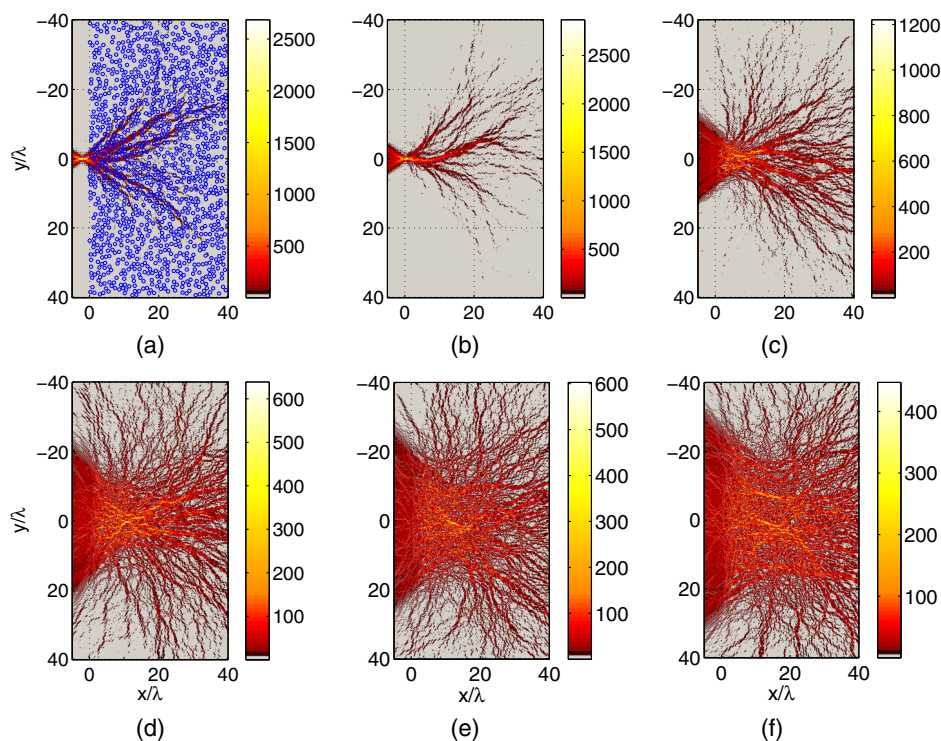


Fig. 2 The intensity (W/m^2) of a focused beam at different focus positions ($\theta_{\text{max}} = 45$ deg). The upper left picture shows the scatterers in blue, while they are omitted in the other pictures for better visibility of the beam shape. The refractive indices are $n_m = 1.33$, and $n_s = 1.5$. x_0 is the focal position. (a) $x_0/\lambda = -2.5$, (b) $x_0/\lambda = 0$, (c) $x_0/\lambda = 9$, (d) $x_0/\lambda = 18$, (e) $x_0/\lambda = 23$, and (f) $x_0/\lambda = 28$.

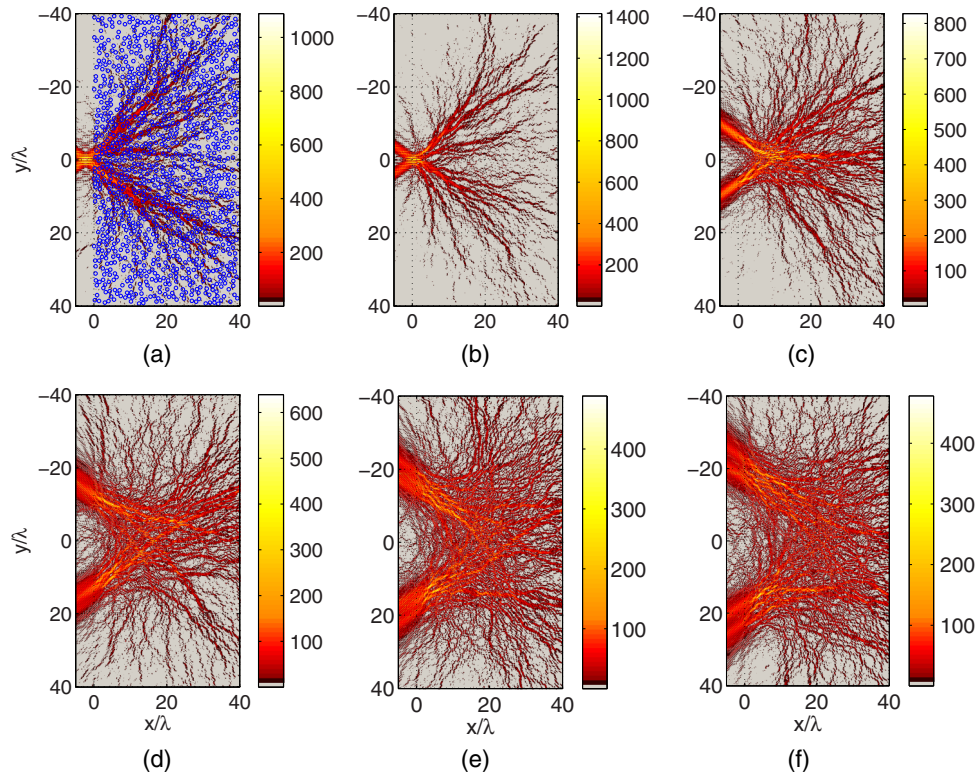


Fig. 3 The intensity (W/m^2) of a quasi-Bessel beam at different focus positions ($\theta_{max} = 45$ deg, $\Delta\theta = 20$ deg). The upper left picture shows the scatterers in blue, while they are omitted in the other pictures for better visibility of the beam shape. The origin in the longitudinal direction is placed at the starting point of the scatterers. The refractive indices are $n_m = 1.33$, and $n_s = 1.5$. x_0 is the focal position. (a) $x_0/\lambda = -2.5$, (b) $x_0/\lambda = 0$, (c) $x_0/\lambda = 9$, (d) $x_0/\lambda = 18$, (e) $x_0/\lambda = 23$, and (f) $x_0/\lambda = 28$.

of both the scatterers and the surrounding is used to get the approximate new position of the focus:

$$x_0 = \hat{x}_0 \frac{n_m C_m + n_s C_s}{n_m}, \quad (6)$$

where the factors used in the correction term (C_s and C_m) are the fractional area of the scatterers and the surrounding medium, respectively. Figure 7 shows the lateral intensity of each beam at different depths to see the deterioration of the beam profile. In Fig. 8, two sizes of cylindrical scatterers are used to investigate the dependence of the on-axis intensity on the size of the scatterers while maintaining the same volume concentration.

5 Discussion

Obviously, for a given distribution of the scatterers, the penetration depth depends mainly on the scattering properties of the considered medium. However, it is interesting to note that the rate of change of the transmission channels seen in Figs. 2 and 3 depends heavily on the type of beam. For the focused beam (Fig. 2), a shift of $1 \mu m$ ($x_{sh} = 1 \mu m$) is enough to change the transmission channels considerably (not shown). In the case of the quasi-Bessel beam on the other hand (Fig. 3), the focus can be shifted by $10 \mu m$ and still mostly retain the same transmission channels. After the incoherent averaging in Figs. 4 and 5, it is easier to study the decrease of the beam intensity versus

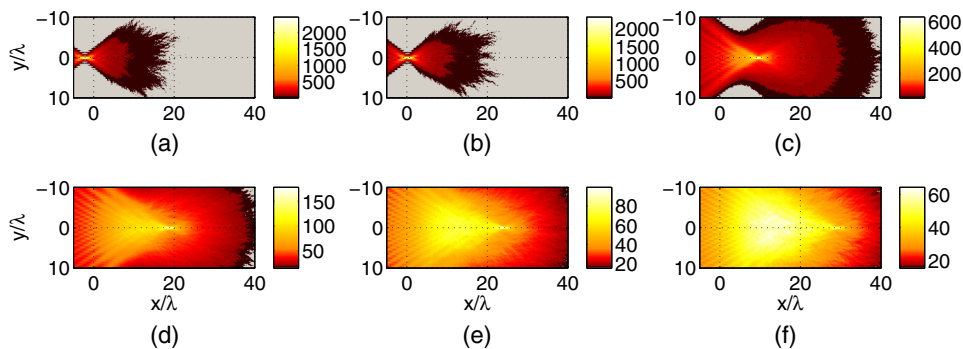


Fig. 4 The intensity (W/m^2) for the focused beam in Fig. 2, averaged over a lateral range. x_0 is the focal position. (a) $x_0/\lambda = -2.5$, (b) $x_0/\lambda = 0$, (c) $x_0/\lambda = 9$, (d) $x_0/\lambda = 18$, (e) $x_0/\lambda = 23$, and (f) $x_0/\lambda = 28$.

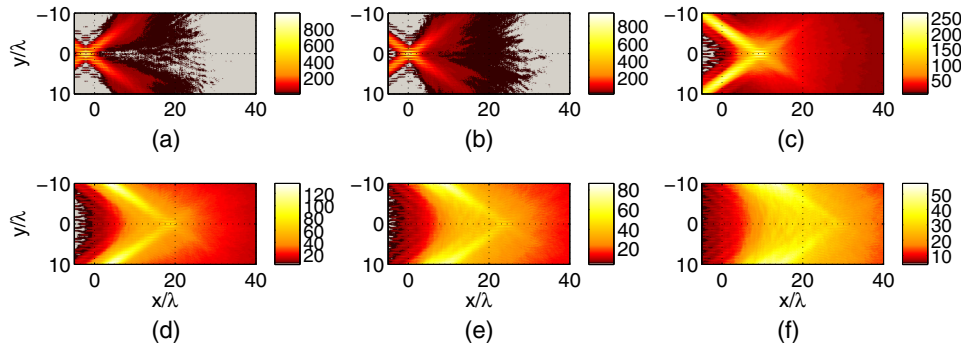


Fig. 5 The intensity (W/m^2) for the quasi-Bessel beam in Fig. 3, averaged over a lateral range. x_0 is the focal position. (a) $x_0/\lambda = -2.5$, (b) $x_0/\lambda = 0$, (c) $x_0/\lambda = 9$, (d) $x_0/\lambda = 18$, (e) $x_0/\lambda = 23$, and (f) $x_0/\lambda = 28$.

depth. Furthermore, the channels that could be seen before in Figs. 2 and 3 disappear. This indicates, as expected, that such channels depend on the individual distribution of the scatterers.

By adding the intensity of the two beams corresponding to the angular ranges of $|\theta| = [0 \text{ deg} : 25 \text{ deg}]$ and $|\theta| = [25 \text{ deg} : 45 \text{ deg}]$ in Fig. 6, we observe that it is approximately equal to the intensity of the beam in the range of $|\theta| = [0 \text{ deg} : 45 \text{ deg}]$ at the surface of the sample. This is due to the fact that each beam is normalized to the same incident differential power, and for the beam in the range of $|\theta| = [0 \text{ deg} : 45 \text{ deg}]$, we get about double the intensity of the arithmetic mean of the two beams in the ranges of $|\theta| = [0 \text{ deg} : 25 \text{ deg}]$ and $|\theta| = [25 \text{ deg} : 45 \text{ deg}]$ because of the coherent addition of the plane waves. By going deeper into the sample, the light experiences more scattering interactions and less constructive interference occurs in the focal region due to the decreasing nonscattered part of the light. As a result, we find that the intensity of the beam in the range of $|\theta| = [0 \text{ deg} : 45 \text{ deg}]$ equals the arithmetic mean of the intensities of the beams in the ranges of $|\theta| = [0 \text{ deg} : 25 \text{ deg}]$ and $|\theta| = [25 \text{ deg} : 45 \text{ deg}]$.

Usually, a beam with a larger maximum divergence angle has a tighter focus. Since all the simulated beams have the same incident differential power, the more focused beam has higher

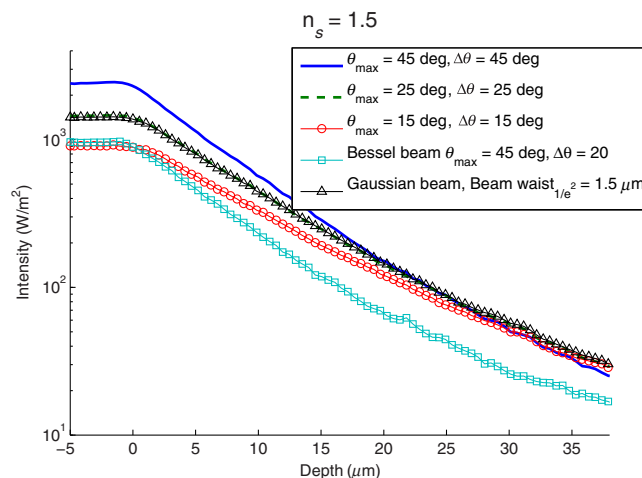


Fig. 6 The on-axis intensity for the focused, Gaussian, and quasi-Bessel beams for the same incident differential power. The refractive indices are $n_m = 1.33$ and $n_s = 1.5$.

intensity at the focus. This can be seen in, e.g., Fig. 7 at the depth of $-2.5 \mu\text{m}$. This changes when the beams propagate through the scattering medium. At higher depths, the high numerical aperture (NA) beams lose their advantage of having higher intensity at the focus to some extent. This can be visualized by looking at the propagation path of the individual plane waves that make up these beams. For the focused beam with $\theta_{\text{max}} = 45 \text{ deg}$, the most divergent plane waves propagate a longer distance in the scattering medium due to their more oblique propagation directions and thus, they are more attenuated and comparable to the plane waves which are incident at smaller angles. This also explains the good performance of the Gaussian beam, which has most of its power in the small angles, while the quasi-Bessel beam shows a disadvantage in this case since relatively large angles are applied. In addition, using low NA beams proves more efficient because it avoids the unnecessary illumination of the sample with the light coming from the large incident angles, which prevents, e.g., bleaching in biological samples. We note that it is not so common to have a Bessel beam which is strongly focused, since the most attractive feature of such a beam is the large depth of field.¹⁰ However, our purpose here is to examine the basics of the propagation of such a beam. Also, since we are only simulating in 2-D, we do not have the option of simulating a real Bessel beam since it will simply appear as a sinusoidal wave.

As can be seen in Fig. 7, the intensity at y -values outside the beam focus area keeps rising at different rates for each of the simulated beams when the focus depth is increased. This “background” intensity is caused by multiple scattered light. Thus, it also affects the decrease rate of the curves in Fig. 6 making it difficult to judge where and if the intensity curves of different beams, which are only due to the nonscattered light, intersect.

In order to study only the nonscattered contribution to the intensity at the focus area versus depth, the following analytical equation was applied:

$$E_s(x, y, \mu_s) = \int_{-\theta_{\text{max}}}^{\theta_{\text{max}}} \hat{E}(\theta) \exp\left(-\frac{1}{2}\mu_s \frac{x}{\cos \theta}\right) \times \exp[jk(x \cos \theta + y \sin \theta)] \sqrt{\cos \theta}. \quad (7)$$

In Eq. (7), a Beer–Lambert exponential term is added to the ASPW expression of Eq. (1) to take into account the decrease in intensity due to scattering in a medium with a certain μ_s .

We validated this model by comparing its results to those obtained with the FDTD method. Three more FDTD

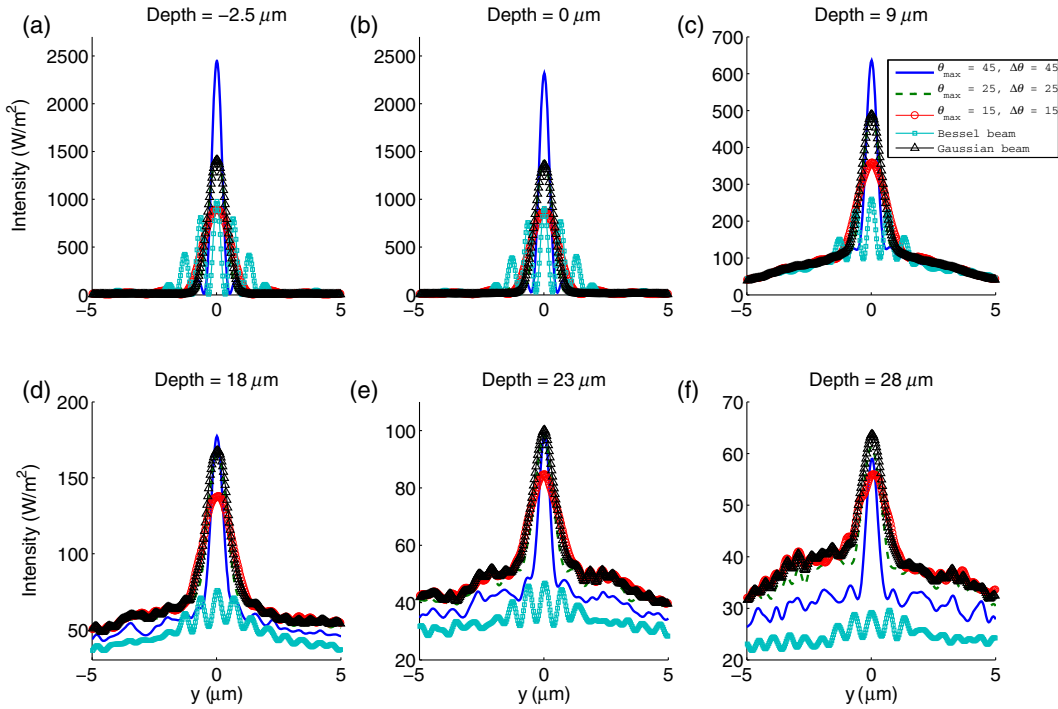


Fig. 7 The lateral profile of the beams at different depths for $n_m = 1.33$ and $n_s = 1.5$. The differential power of each incident beam is equal to 1 W/m . The quasi-Bessel beam has $\theta_{\max} = 45$ deg and $\Delta\theta = 20$ deg, while the Gaussian beam has a FWHM = $0.86 \mu\text{m}$. (a) Depth = $-2.5 \mu\text{m}$, (b) depth = $0 \mu\text{m}$, (c) depth = $9 \mu\text{m}$, (d) depth = $18 \mu\text{m}$, (e) depth = $23 \mu\text{m}$, and (f) depth = $28 \mu\text{m}$.

simulations were run ($n_s = 1.4, 1.5,$ and 1.9 in $n_m = 1.33$ corresponding to $\rho = 117, 19.8,$ and $3.4 \mu\text{m}$, respectively) using a lower volume concentration of 5% for cylinders with diameter of $1 \mu\text{m}$. This was done to decrease the influence of the dependent scattering. The analytical model shows good agreement to the FDTD simulations at low scattering ($\rho = 117$ and $19.8 \mu\text{m}$). For the higher scattering ($\rho = 3.4 \mu\text{m}$), the curves started showing significant differences due to dependent scattering. The beams profile at three different depths calculated with Eq. (7) can be seen in Fig. 9 for similar scattering parameters as in Fig. 7 ($\rho = 3.84 \mu\text{m}$) but for a lower concentration

(conc. = -5%). As an advantage of using this model, we can investigate the focus due to the nonscattered light much deeper in the scattering medium than is possible with the FDTD method, compare to Fig. 7. From Fig. 9, we can see that the deeper the focus depth, the more the widths of the beams are broadening and the more the profiles of the different beams approach each other as expected from Fig. 7. This is due to the smaller contribution of the plane waves incident at larger angles. Figure 10 shows the intensity ratio of the beams with θ_{\max} of 25 deg to θ_{\max} of 45 deg for the same scattering medium. It can be seen that for depths larger than $25.7 \mu\text{m}$, the intensity of the smaller NA beam is larger than that for the larger NA

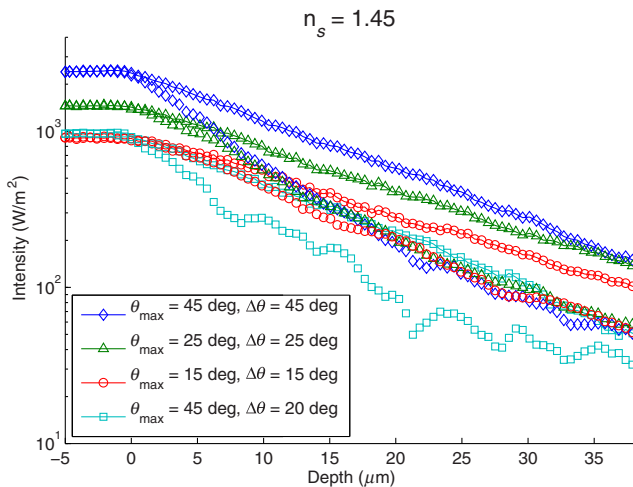


Fig. 8 The on-axis intensity for the beams using two sizes of cylindrical scatterers ($d = 1 \mu\text{m}$ for symbols with lines and $2 \mu\text{m}$ for symbols only) while n_s is kept equal to 1.45 .

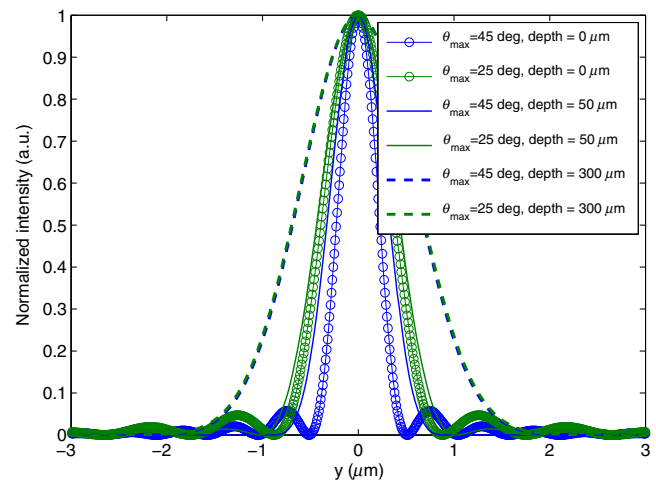


Fig. 9 Beam profiles at three different depths using the analytical solution for the nonscattered light ($\rho = 3.4 \mu\text{m}$).

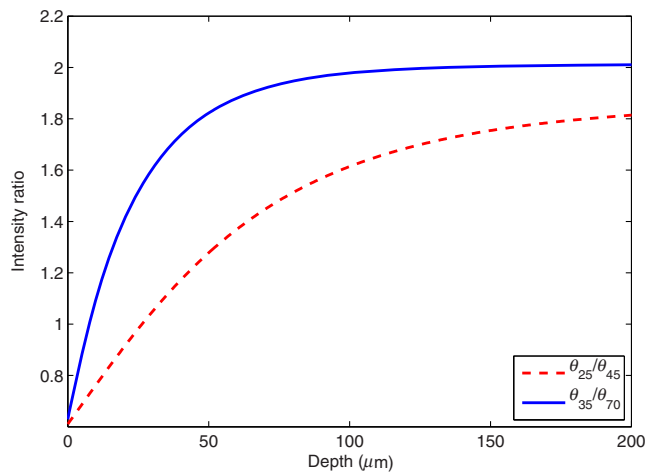


Fig. 10 Ratio of the intensities for different beams using the analytical solution for the nonscattered light for the case when ρ is equal to $3.4 \mu\text{m}$.

beam. Thus, at large depths not only the total intensity at the focus position is larger for smaller θ_{max} compared to larger θ_{max} but also the intensity due to nonscattered light. Figure 10 shows, in addition, the intensity ratio of the focused beams with θ_{max} of 35 deg to θ_{max} of 70 deg. In this case, for depths larger than about $8 \mu\text{m}$, the nonscattered intensity of the smaller NA beam is larger than that of the larger NA beam. We note that a maximal incident angle of 70 deg corresponds to very high NA objective used in practice.¹

Due to the large hardware resources needed for the FDTD method, we simulated the light propagation only in a relative small area. Therefore, we used scattering objects which have large scattering coefficients. This restriction can be released when the analytical equation is used allowing the use of more realistic optical properties for biomedical tissues. Thus, using a typical scattering coefficient which is, e.g., 10 times lower than is applied in Fig. 10, it follows that the shown curves are also scaled by a factor of 10. This means that the depths, where the intensity ratio is 1, are also a factor of 10 larger. For example, it follows that the intensity of the nonscattered light of a relative low NA beam with θ_{max} of 35 deg is larger than that of a high NA beam with θ_{max} of 70 deg for depths larger than about $80 \mu\text{m}$. However, we also note that the depth where the lateral profiles of the beam approach each other is increased (in the above case at about $800 \mu\text{m}$).

The previously mentioned conclusions that came from applying Eq. (7) can be generalized to the 3-D case. However, special care needs to be taken by adding an extra vector to the equation to control the polarization of the beam.²⁵ Figure 11 shows the 3-D results corresponding to the 2-D results shown in Fig. 10. It is interesting to note that we see the same phenomena of intensity enhancement when using a low NA beam in comparison to the high NA case. Of course, it should be noted that in this case, we have to consider solid angles since we are dealing with the 3-D setup. This is the reason for the higher intensity enhancement found in Fig. 11 when compared to Fig. 10 despite having the same ratio between the divergence angles in both cases.

As a rule of thumb, the scattering cross section increases with the size of the scatterer.²⁷ This can be seen in Fig. 8, where the on-axis intensity for the larger scatterers ($d = 2 \mu\text{m}$) decreases at a higher rate than the case of smaller scatterers ($d = 1 \mu\text{m}$).

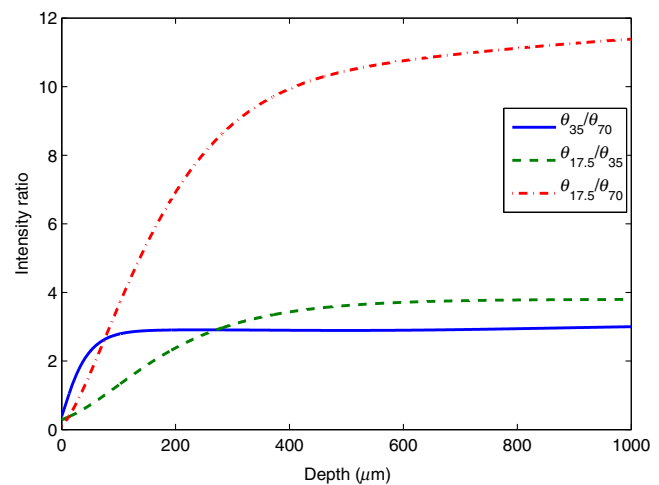


Fig. 11 Ratio of the intensities for different beams using the analytical solution for the nonscattered light for the case when ρ is equal to $3.4 \mu\text{m}$ in 3-D.

This also agrees with the analytical solution of the scattering of a plane wave by a cylinder²⁷ since for the bigger cylinder ($d = 2 \mu\text{m}$), we obtain a scattering cross section C_{scat} of $2.7 \mu\text{m}$, whereas for the smaller cylinder ($d = 1 \mu\text{m}$), C_{scat} is $0.39 \mu\text{m}$. Comparing the results presented in Fig. 8, it can be seen that the efficiency of the averaging is worse for the cylinders with a larger diameter. This is mainly because of the higher correlation of the results obtained in the case of the larger scattering objects due to the smaller ratio of the lateral beam shifts to the cylinder diameter.

6 Conclusion

In this study, the propagation of several types of beams through scattering materials was investigated. Focused, Gaussian, and quasi-Bessel beams were simulated in 2-D. The study was performed by numerically solving Maxwell's equations using the FDTD method. Solutions of Maxwell's equations are superior to Monte Carlo simulations because all effects of classical physics such as dependent scattering are included.²⁹ The incident beams were modeled using the ASPW method, which enables the manipulation of the phases of the individual plane waves that constitute the modeled beam. The simulation of the scanning of the beams is achieved in an efficient way¹⁷ both in the axial direction (to study the effect of depth scanning on the quality of the beam focus) and in the lateral direction (which allows for an effective averaging technique).

The results show that for focusing light in scattering media, the focus intensity of a high NA beam decreases faster versus depth than is the case for a small NA beam. The FDTD simulations demonstrate that at a certain depth in the scattering medium, the total intensity at the focus position (including both the nonscattered and the scattered light) is larger, e.g., for the $\theta_{\text{max}} = 25$ deg focused beam compared to the $\theta_{\text{max}} = 45$ deg focused beam. However, due to the high amount of necessary calculation time (for large depths and, thus, large simulation areas), the FDTD simulations do not show if this is also the case for the focus intensity of the nonscattered light, which is the important quantity for many microscopical applications. Here, we used a simple mathematical model to calculate the intensity profile for the nonscattered light versus depth and lateral positions. It shows that for large depths, the focus intensity of the

nonscattered light is larger for the low NA beam than for the high NA one, e.g., about twice as large for the $\theta_{\max} = 25$ deg focused beam compared to the $\theta_{\max} = 45$ deg focused beam. In addition, we showed that for a large focus depth, the lateral profile of the nonscattered intensity of the low NA beams approaches that of the high NA beams resulting in a similar resolution when used in a microscope.

In summary, for microscopical applications deep in a scattering medium, the use of beams with a lower NA can be advantageous compared to higher NA beams. Finally, we note that the models used in this study can be readily extended from the 2-D to the 3-D case, where it is expected that the advantages of the low NA beams are even greater.

Acknowledgments

This research has been supported by the Baden-Württemberg Stiftung, and the Evangelisches Studienwerk e.V. Villigst. Special thanks to our colleague Julian Stark for all the fruitful discussions.

References

- W. Denk, J. H. Strickler, and W. W. Webb, "Two-photon laser scanning fluorescence microscopy," *Science* **248**, 73–76 (1990).
- J. M. Schmitt, A. Knüttel, and M. Yadlowsky, "Confocal microscopy in turbid media," *J. Opt. Soc. Am. A* **11**, 2226–2235 (1994).
- A. Knüttel, S. Bonev, and W. Knaak, "New method for evaluation of in vivo scattering and refractive index properties obtained with optical coherence tomography," *J. Biomed. Opt.* **9**, 265–273 (2004).
- D. Roy, "Two-photon scattering of a tightly focused weak light beam from a small atomic ensemble: an optical probe to detect atomic level structures," *Phys. Rev. A* **87**, 063819 (2013).
- G. Wang and J. F. Webb, "Calculation of electromagnetic field components for a fundamental Gaussian beam," *Phys. Rev. E* **72**(4), 046501 (2005).
- F. O. Fahrbach and A. Rohrbach, "A line scanned light-sheet microscopy with phase shaped self-reconstructing beams," *Opt. Express* **18**(23), 24229–24244 (2010).
- B. Richards and E. Wolf, "Electromagnetic diffraction in optical systems. II. Structure of the image field in an aplanatic system," *R. Soc. London Proc. Ser. A* **253**, 358–379 (1959).
- G. P. Agrawal and D. N. Pattanayak, "Gaussian beam propagation beyond the paraxial approximation," *J. Opt. Soc. Am.* **69**(4), 575–578 (1979).
- F. O. Fahrbach et al., "Light-sheet microscopy in thick media using scanned Bessel beams and two-photon fluorescence excitation," *Opt. Express* **21**(11), 13824–13839 (2013).
- F. O. Fahrbach et al., "Self-reconstructing sectioned Bessel beams offer submicron optical sectioning for large fields of view in light-sheet microscopy," *Opt. Express* **21**(9), 11425–11440 (2013).
- T. Čížmár et al., "Generation of multiple Bessel beams for a biophotonics workstation," *Opt. Express* **16**(18), 14024–14035 (2008).
- L. C. Thomson and J. Courtial, "Holographic shaping of generalized self-reconstructing light beams," *Opt. Commun.* **281**(5), 1217–1221 (2009).
- T. Čížmár and K. Dholakia, "Tunable Bessel light modes: engineering the axial propagation," *Opt. Express* **17**(18), 15558–15570 (2009).
- M. D. Feit and J. A. Fleck Jr., "Light propagation in graded-index optical fibers," *Appl. Opt.* **17**(24), 3990–3998 (1978).
- A. Rohrbach, "Artifacts resulting from imaging in scattering media: a theoretical prediction," *Opt. Lett.* **34**(19), 3041–3043 (2009).
- İ. R. Çapoğlu, A. Taflove, and V. Backman, "Generation of an incident focused light pulse in FDTD," *Opt. Express* **16**(23), 19208–19220 (2008).
- A. Elmaklizi, J. Schäfer, and A. Kienle, "Simulating the scanning of a focused beam through scattering media using a numerical solution of Maxwell's equations," *J. Biomed. Opt.* **19**(7), 071404 (2014).
- İ. R. Çapoğlu, A. Taflove, and V. Backman, "Computation of tightly focused laser beams in the FDTD method," *Opt. Express* **21**(1), 87–101 (2013).
- F. O. Fahrbach, P. Simon, and A. Rohrbach, "Microscopy with self-reconstructing beams," *Nat. Photonics* **4**(11), 780–785 (2010).
- J. W. Goodman, Chapter 1 in *Introduction to Fourier Optics*, 3rd ed., Roberts and Company Publishers, Greenwood Village, CO (2005).
- L. Novotny and B. Hecht, Chapter 3 in *Principles of Nano-Optics*, Cambridge University Press, Cambridge, United Kingdom (2006).
- J. Schäfer et al., FDTD-simulation of multiple light scattering in dentin, in *Biomedical Topical Meeting*, p. SH60, Optical Society of America (2006).
- S. Kozaki, "Scattering of a Gaussian beam by a homogeneous dielectric cylinder," *J. Appl. Phys.* **53**(11), 7195–7200 (1982).
- J. Lin et al., "Cosine-Gauss plasmon beam: a localized long-range nondiffracting surface wave," *Phys. Rev. Lett.* **109**(9), 093904 (2012).
- A. Taflove and S. C. Hagness, *Computational Electrodynamics: The Finite Difference Time-Domain Method*, 3rd ed., Artech House, Norwood, MA (2005).
- L. Roux et al., "Scattering by a slab containing randomly located cylinders: comparison between radiative transfer and electromagnetic simulation," *J. Opt. Soc. Am. A* **18**(2), 374–384 (2001).
- C. F. Bohren and D. R. Huffman, Chapter 8 in *Absorption and Scattering of Light by Small Particles*, Wiley-Interscience Publication, Hoboken, NJ (1940).
- S. H. Tseng, "2-D PSTD simulation of focusing monochromatic light through a macroscopic scattering medium via optical phase conjugation," *Biomed. Opt. Express* **6**(3), 815–826 (2015).
- W. Jie et al., "Influence of numerical aperture on focal spot in turbid media microscopy," in *2nd Int. Congress IEEE Image and Signal Processing*, pp. 1–4 (2009).

Ahmed Elmaklizi is a PhD student at the Institut für Lasertechnologien in der Medizin und Meßtechnik (ILM), Ulm, Germany, and part of the materials optics and imaging group at ILM. He got his BSc degree in electrical engineering from the German University in Cairo (GUC), and got his master of science degree in communication engineering from University of Ulm.

Dominik Reitzle is a PhD student at the Institut für Lasertechnologien in der Medizin und Meßtechnik (ILM), Ulm, Germany, and part of the materials optics and imaging group at ILM. He studies physics at the University of Ulm.

Arnd Brandes completed his bachelor's degree in information technology (BE) in 2009 and his master's degree in biomedical engineering (ME) in 2010. Since then he has been working as a PhD student in the material optics and imaging group under supervision of Alwin Kienle, and since 2015 as a development engineer at Cubert GmbH.

Alwin Kienle is a vice director (science) of the Institut für Lasertechnologien in der Medizin und Meßtechnik (ILM), Ulm, Germany, and head of the materials optics and imaging group at ILM. In addition, he is a professor at the University of Ulm. He studied physics and received his doctoral and habilitation degrees from the University of Ulm. As a postdoc, he worked with research groups in Hamilton, Canada, and Lausanne, Switzerland.